Journal of Luminescence 247 (2022) 118867

Contents lists available at ScienceDirect

Journal of Luminescence

journal homepage: www.elsevier.com/locate/jlumin

Divalent and trivalent neodymium photoluminescence in $NaMgF_3$:Nd

J.J. Schuyt [a,*], G.V.M. Williams [b]

[a] Robinson Research Institute, Victoria University of Wellington, PO Box 33436, Lower Hutt 5046, New Zealand
[b] The MacDiarmid Institute for Advanced Materials and Nanotechnology, SCPS, Victoria University of Wellington, PO Box 600, Wellington 6140, New Zealand

ARTICLE INFO

Keywords:
$NaMgF_3$
Neodymium
Radiophotoluminescence
Luminescent electron traps

ABSTRACT

Photoluminescence from Nd^{3+} and Nd^{2+} ions was observed in polycrystalline $NaMgF_3$:Nd synthesised via a high-temperature melt, slow-cooling technique. The spectral features of Nd^{3+} were directly attributed to known intraconfigurational $4f^3 \rightarrow 4f^3$ transitions, where numerous emissions occurred in the infrared spectral region 840 nm–1390 nm. Additional emissions were observed over the range 850 nm–1500 nm that could not be attributed to Nd^{3+}. The additional emissions were attributed to specific intraconfigurational $4f^4$ transitions of Nd^{2+} via comparison of the photoluminescence features with the known transitions of the isoelectronic Pm^{3+} ion in similar host compounds. The energies of the Nd^{2+} $4f^4$ levels were compressed by a factor of 1.09 relative to the Pm^{3+} ion. X-ray irradiation produced a radiophotoluminescence effect whereby the Nd^{2+} emission intensities increased for optical stimulations below 450 nm. Continuous stimulation at 400 nm reversed this effect. This phenomenon could be useful for applications in infrared lasing, radiation detection, and optical information storage.

1. Introduction

The series of lanthanides (Ln), comprised of the elements lanthanum through lutetium, possess distinct magnetic and optical properties that have provided the basis for numerous technologies, including lasers [1], light-emitting diodes [2,3], scintillators [3,4], biological imaging nanoparticles [3,5] and electric motors [6]. The properties of the Ln elements are primarily determined by their electronic configurations, i.e., by the number, n, of electrons in the $4f$ orbitals, where the partial filling of these orbitals can produce very high magnetic moments [6] and rich electronic structures [7,8]. The $4f^n$ electrons are well-shielded from external environments and are not strongly influenced by crystal field effects [9]. Consequently, the $4f^n$ energy levels of the various Ln ions, when incorporated into different host compounds, are very similar to those of the free Ln ions. All Ln form trivalent ions, Ln^{3+}, and the optical and magnetic properties of Ln^{3+} ions have been studied in many thousands of host compounds [9,10]. As divalent Ln ions (Ln^{2+}) are significantly less stable than their Ln^{3+} counterparts, analyses of the various Ln^{2+} ions are lacking in comparison [9,11]. The notable exceptions to this rule are Eu^{2+}, Sm^{2+}, and Yb^{2+}, which are commonly observed in a range of materials [12–16]. It is of interest to study the remaining series of Ln^{2+}, due in part to their more readily accessible $4f^{n-1}5d$ orbitals that are strongly affected by crystals fields, and their potential electron trapping properties in insulating materials [17,18].

Recent research evaluating the luminescence properties of Ln-doped $NaMgF_3$ has revealed that the fluoroperovskite host is an excellent model compound through which spectral information on various divalent lanthanides may be obtained [19–23]. In some cases, mixed valence luminescence from both divalent and trivalent lanthanides is observed in as-made samples, as with Sm-, Yb-, and Eu- doped $NaMgF_3$ [19,20]. Additionally, exposure of the compound to X-ray irradiation often causes the reduction $Ln^{3+} \rightarrow Ln^{2+}$, allowing photoluminescence studies of uncommon Ln^{2+} ions to be performed, as was recently reported for the $NaMgF_3$:Dy compound [21]. The host-referred binding energy (HRBE) diagram for the various $NaMgF_3$:Ln systems suggests that a range of additional Ln^{2+} ions, including Pr^{2+}, Nd^{2+}, Ho^{2+}, Er^{2+}, and Tm^{2+} will be stable in the host after X-ray exposure [19]. Of particular interest is the Nd^{2+} ion, due in part to its rich $4f^4$ electronic structure that allows optical transitions ranging from the visible to the infrared that could be used for infrared lasing [24,25]. Additionally, Nd^{2+} is isoelectronic to the highly unstable and seldom studied Pm^{3+} ion [24–26], and a relative lack of spectral information is currently available for both Pm^{3+} and Nd^{2+} ions, encouraging attempts to better characterise the luminescence properties of Nd^{2+}.

Nd^{2+} luminescence has been observed in very few compounds thus far. Like many divalent lanthanides, Nd^{2+} has a proclivity to oxidise to

* Corresponding author.
E-mail address: joe.schuyt@vuw.ac.nz (J.J. Schuyt).

https://doi.org/10.1016/j.jlumin.2022.118867
Received 17 November 2021; Received in revised form 23 February 2022; Accepted 26 March 2022
Available online 28 March 2022

the trivalent state, where the Nd^{3+}/Nd^{2+} reduction potential is −2.62 V in aqueous solution [9]. Consequently, it is expected that Nd^{2+} can only be stabilised in very wide-bandgap compounds ($\varepsilon_g \approx 10$ eV). To our knowledge, spectroscopic data related to Nd^{2+} have thus far been presented only for CaF_2:Nd [27,28], SrF_2:Nd [28], BaF_2:Nd [28], LiCl–KCl melts [29], SrB_4O_7:Nd [30], $SrCl_2$:Nd [11,31], SrI_2:Nd and $SrBr_2$:Nd [32], and $KMgF_3$:Nd [33], in contrast to the several thousands of compounds for which other divalent lanthanides, such as Eu^{2+} [9,12,17], have been studied in detail. In the majority of the aforementioned cases, only $4f^4 \rightarrow 4f^3 5d^1$ absorptions were observed [28–30], precluding any detailed analysis of the various intraconfigurational $4f^4 \rightarrow 4f^4$ transitions. To date, experimental energy levels of the intraconfigurational $4f^4$ transitions have not been presented, and their relation to the energy levels of Pm^{3+} has not been explored in detail.

Here we present a photoluminescence study of $NaMgF_3$:0.5%Nd before and after exposure to X-ray irradiation. We show that the majority of Nd substitutes in the trivalent state, though a fraction of the Nd occupies the divalent state in as-made samples. Via comparison with data available in the literature regarding the electronic structure of Pm^{3+}, we attribute the various excitations and emissions observed from the Nd^{2+} ion to specific electronic transitions. Finally, we show that X-ray exposure results in an optically-reversible increase in the Nd^{2+} emission intensities upon excitation below 450 nm. This radio-photoluminescence (RPL) effect provides a mechanism through which optical and radiation sensing can be performed, and therefore $NaMgF_3$:Nd may find applications in optical information storage and dosimetry.

2. Experimental

Samples of polycrystalline $NaMgF_3$:Nd with a nominal concentration of 0.5 mol% Nd were synthesised via a high-temperature melt technique. Precursor fluorides NaF (Sigma-Aldrich 99.99%), MgF_2 (Sigma-Aldrich ≥99.99%), and NdF_3 (Cerac 99.9%) were mixed in stoichiometric ratios in a low-oxygen low-humidity MBRAUN UNIlab glovebox, subsequently transferred to a Sigradur GAZ2 glassy carbon crucible, and placed in a custom-built RF furnace in an Ar atmosphere. The mixture was then heated to 1100 °C over 1 h, cooled to 1035 °C over 1 h, then slow-cooled through the melting point of $NaMgF_3$ to 1015 °C over 12 h. The sample was then left to cool to room temperature prior to retrieval. Transparent pieces were then cut from the sample with dimensions of approximately 5 mm × 5 mm × 1 mm for further analysis. Photoluminescence measurements were performed using a Jobin-Yvon Fluorolog-3 spectrofluorometer where the spectra were corrected for variations in the excitation intensities. X-ray irradiations were performed using a modified Philips PW1730 X-ray generator with a W tube operated at 40 kV and 20 mA. The X-ray beam was hardened using a 0.9 mm Al filter, such that the average X-ray energy was 24.7 keV and the approximate absorbed dose rate at the sample surface was 0.1 Gy s^{-1}.

3. Results and discussion

Photoluminescence spectra of the as-made $NaMgF_3$:Nd sample are shown in Fig. 1, where the major excitations and emissions occurred due to the presence of Nd^{3+} ions. Based on previous studies of $NaMgF_3$:Ln materials, it is expected that the Nd^{3+} ions substitute the Na^+ sites of the $NaMgF_3$ host [34–36]. This interpretation is reinforced by the relevant ionic radii, where in 8-fold coordination the ionic radii of Nd^{3+} and Na^+ are 1.11 Å and 1.18 Å, respectively [37]. In contrast, the Mg^{2+} site in 6-fold coordination has ionic radius 0.72 Å and the Nd^{3+} ion in the same coordination has ionic radius 0.98 Å [37], such that the substitution of Nd^{3+} for Mg^{2+} is unlikely as a significant lattice distortion would be required to incorporate the dopant. As the substitution $Nd^{3+} \leftrightarrow Na^+$ requires charge compensation, additional defects must be incorporated into the lattice, likely in the form of O^{2-} impurities and Na^+ vacancies [38,39]. The presence of these defects produces multiple Nd^{3+} sites with distinct crystalline environments leading to slightly different optical transition energies, though the small influence of crystal fields on $4f^n \leftrightarrow 4f^n$ transitions results in only minor splitting or broadening of the excitation and emission bands.

Fig. 1(a) shows the emission spectrum of the $NaMgF_3$:Nd compound where $\lambda_{ex} = 575$ nm. Three infrared emission clusters were observed, spanning 840 nm–945 nm, 1000 nm–1140 nm, and 1275 nm–1390 nm. The $\lambda_{ex} = 575$ nm stimulation excited the Nd^{3+} electrons from the $^4I_{9/2}$ ground state to the $^4G_{5/2}$, $^2G_{7/2}$ excited states, after which the electrons non-radiatively decayed to the $^4F_{3/2}$ level, prior to radiative decay to the $^4I_{9/2}$, $^4I_{11/2}$, and $^4I_{13/2}$ levels that produced the three emissions bands in order of decreasing energy. Fig. 1(b) shows the excitation spectrum where $\lambda_{em} = 1061$ nm, corresponding to the peak of the aforementioned $^4F_{3/2} \rightarrow {}^4I_{11/2}$ emissions. Various line excitations were observed over the range of wavelengths accessible to the spectrometer, from approximately 300 nm–800 nm, all of which are readily attributed to intraconfigurational $4f^3 \rightarrow 4f^3$ transitions of Nd^{3+}. The large number of excitation energies available in the production of Nd^{3+} infrared emissions may be useful in any context where infrared emissions are desirable, e.g., infrared lasing. As there are several possible transitions via which the Nd^{3+} ion can relax from the various excited states to the $^4I_{9/2}$ ground state, it was of interest to observe whether any evidence of quantum cutting, a form of downconversion, was present in the $NaMgF_3$:Nd spectra [40]. For example, multiple radiative decays could occur via excitation into the $^4G_{9/2}$ level (e.g. $^4G_{9/2} \rightarrow {}^4F_{3/2} \rightarrow {}^4I_{9/2}$, yielding two photons at 1170 nm and 900 nm). However, exciting into higher energy levels did not produce any new emissions over the wavelength region

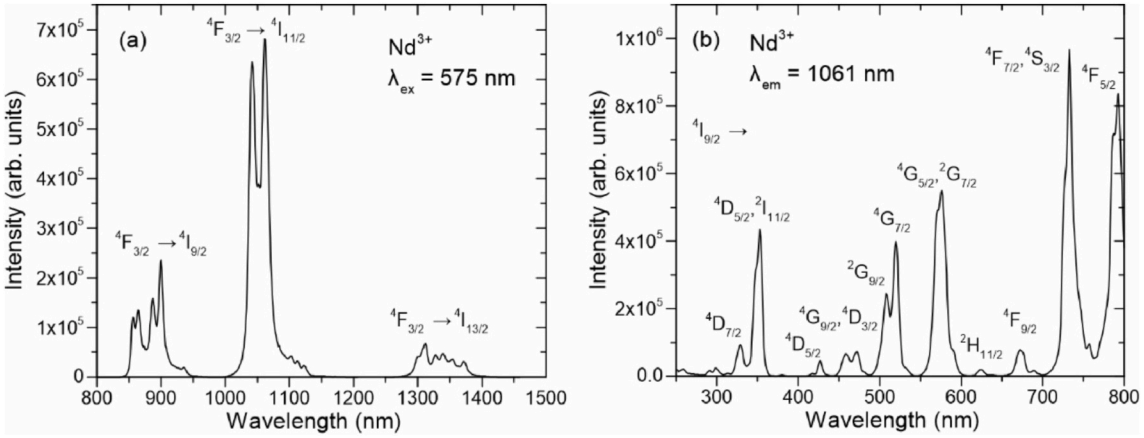

Fig. 1. (a) Photoluminescence emission spectrum of $NaMgF_3$:Nd where $\lambda_{ex} = 575$ nm. (b) Photoluminescence excitation spectrum of $NaMgF_3$:Nd where $\lambda_{em} = 1061$ nm.

studied.

While it was expected that Nd^{3+} could be reduced to Nd^{2+} in $NaMgF_3$:Nd via stimulation with ionising radiation, whereby conduction band electrons would be trapped by Nd^{3+} ions, it was of interest to determine whether any Nd^{2+} existed in the as-made samples. An attempt to resolve additional weak luminescence features was performed by systematically varying the PL excitation and emission wavelengths across the wide spectral range 300 nm–1500 nm, and subsequently refining the selected wavelengths in order to maximise the luminescence intensities of all features that could not be attributed to Nd^{3+}. Fig. 2(a) shows the PL emission spectrum where $\lambda_{ex} = 595$ nm, for which multiple line emissions were observed in the range 800 nm–1500 nm that do not resemble those emissions previously attributed to Nd^{3+}, though Nd^{3+} emissions were superimposed upon the new emissions. Fig. 2(b) shows the PL excitation spectrum where $\lambda_{em} = 935$ nm, selected as it corresponds to an emission seen in Fig. 2(a) with relatively high intensity, and because the emission wavelength does not significantly overlap the emissions from Nd^{3+}, in comparison to the alternative emissions. The excitation spectrum exhibited transitions attributed to Nd^{3+} superimposed with new excitations that could not be attributed to Nd^{3+}. The relative peak intensities of the new excitations and emissions were less than 10% of those observed in the Nd^{3+} spectra in Fig. 1, suggesting that the luminescent centre incorporates in a significantly lower concentration. The sharp lines are characteristic of $4f^n$ transitions, and resemble the emissions attributed to Nd^{2+} in the irradiated $KMgF_3$:Nd compound [33]. Consequently, these transitions are attributed to intraconfigurational $4f^4 \leftrightarrow 4f^4$ transitions of Nd^{2+}. The ionic radius of Nd^{2+} in the 8-fold configuration is 1.29 Å [37], indicating that it must also substitute for the Na^+ site of the $NaMgF_3$ host. Again, the requirement for charge compensation likely produced multiple Nd^{2+} sites, depending on the configuration of nearby defects, leading to splitting of the various excitation and emission bands.

Fig. 3 summarises the luminescence features of Nd^{3+} and Nd^{2+}. In order to justify the attribution of the additional PL emissions and excitations to Nd^{2+} centres, a comparison of the transition energies was attempted regarding the isoelectronic Pm^{3+} ion. Pm^{3+} is an incredibly challenging ion to study in any detail as all isotopes are highly radioactive [24]. However, Carnall provided a list of transitions and their corresponding energies for the LaF_3:Pm compound [41], and the subsequent analysis and attributions are primarily based on that list, alongside data obtained for the $LaCl_3$ compound [26]. In order to better separate the PL contributions of Nd^{2+} from those of Nd^{3+} (Fig. 3(a)), a PL normalisation and subtraction technique was employed. The PL emission spectra where $\lambda_{ex} = 595$ nm and $\lambda_{ex} = 575$ nm were first normalised to the Nd^{3+} emission peak at 856 nm. The difference spectrum, PL_{ex}(595 nm) – PL_{ex}(575 nm), was then taken (Fig. 3(b)). Similarly, the PL excitation spectra where $\lambda_{em} = 935$ nm and $\lambda_{em} = 900$ nm were normalised to the Nd^{3+} excitation peak at 353 nm, and the difference spectrum, PL_{em}(935 nm) – PL_{em}(900 nm), then taken (Fig. 3 (b)). The resultant spectra showed contributions solely arising from the luminescent centre attributed to Nd^{2+}. The emission and excitation peaks were then obtained from the spectra and the energies were compared to those of Pm^{3+}, as shown in Table 1.

All emissions and excitations energies observed in Fig. 3(b) correlate with those observed in Pm^{3+}, compressed by 1.09×, as shown in Fig. 3 (c). The compression was expected based on the relative nuclear charges of the Pm and Nd ions. While Pm^{3+} and Nd^{2+} possess the same electronic configuration ($4f^4$), the lower nuclear charge of the Nd ion results in a reduced spin-orbit coupling strength, decreasing the energies of the various $4f^4$ levels in Nd^{2+} relative to Nd^{3+} [9]. The transitions that produced the various Nd^{3+} and Nd^{2+} emissions and excitations are labelled in Fig. 3(a) and (b), and are also contained in Table 1, along with the Pm^{3+} transitions.

It was of interest to compare the compression (1.09×) of Nd^{2+} relative to Pm^{3+} with other mixed-valence Ln^{3+}/Ln^{2+} systems, in particular for the $NaMgF_3$:Ln compounds, where possible. In the first case, Sm^{2+} and Eu^{3+} are isoelectronic and have been studied in detail in the $NaMgF_3$ host [19,20,42], where the Sm^{2+} $4f^6$ excitations were compressed by 1.12× relative to the Eu^{3+} $4f^6$ excitations. In the second case, Dy^{2+} and Ho^{3+} are isoelectronic, where the Dy^{2+} ion has been studied in the $NaMgF_3$ host [21]. Via comparison with the Ho^{3+} transition energies in the similar fluoroperovskite host $KCaF_3$, and YAG [43,44], the compression of the Dy^{2+} $4f^{10}$ transitions relative to the Ho^{3+} transitions was calculated to be 1.13×. These compression factors are given in Table 2, where the compression factor increased with atomic number and number of 4*f* electrons. The increased compression factor throughout the Ln series correlates with the increased spin-orbit coupling energies (ζ) throughout the series. Using the ζ values for the free Ln^{3+} ions provided by Dieke [8], and taking the ratio $\zeta(Ln_1^{3+})/\zeta(Ln_2^{3+})$ for the isoelectronic Ln_1/Ln_2 pairs, we obtained the following: $\zeta(Pm^{3+})/\zeta(Nd^{3+}) = 1.22$, $\zeta(Eu^{3+})/\zeta(Sm^{3+}) = 1.1$, and $\zeta(Ho^{3+})/\zeta(Dy^{3+}) = 1.14$. It should be noted that the values for the Eu/Sm and Ho/Dy pairs are in close agreement with the compression factors previously discussed, while the disagreement for the Pm/Nd pair may arise from errors in accurately determining ζ for the Pm^{3+} ion. However, further studies of the isoelectronic Ln^{2+}/Ln^{3+} pairs in the $NaMgF_3$ host are required to better understand this correlation.

The revised HRBE diagram for the various $NaMgF_3$:Ln systems predicted that the Nd^{2+} ground state lies 2.73 eV below the $NaMgF_3$ conduction band, suggesting that greater concentrations of Nd^{2+} may be produced via the radiation-induced valence conversion $Nd^{3+} \rightarrow Nd^{2+}$, where Nd^{3+} acts as an electron trap [19,23,45]. In general, the greater

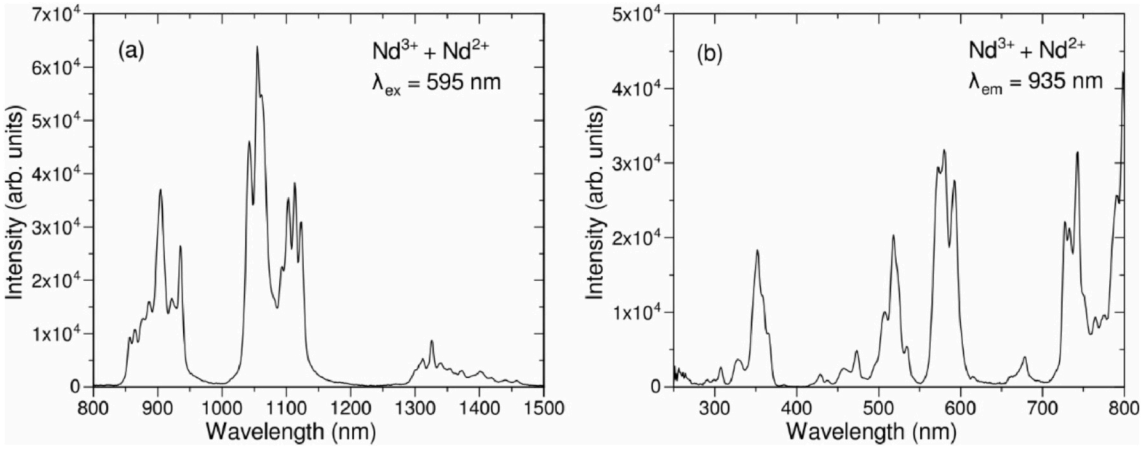

Fig. 2. (a) Photoluminescence emission spectrum of $NaMgF_3$:Nd where $\lambda_{ex} = 595$ nm. (b) Photoluminescence excitation spectrum of $NaMgF_3$:Nd where $\lambda_{em} = 935$ nm.

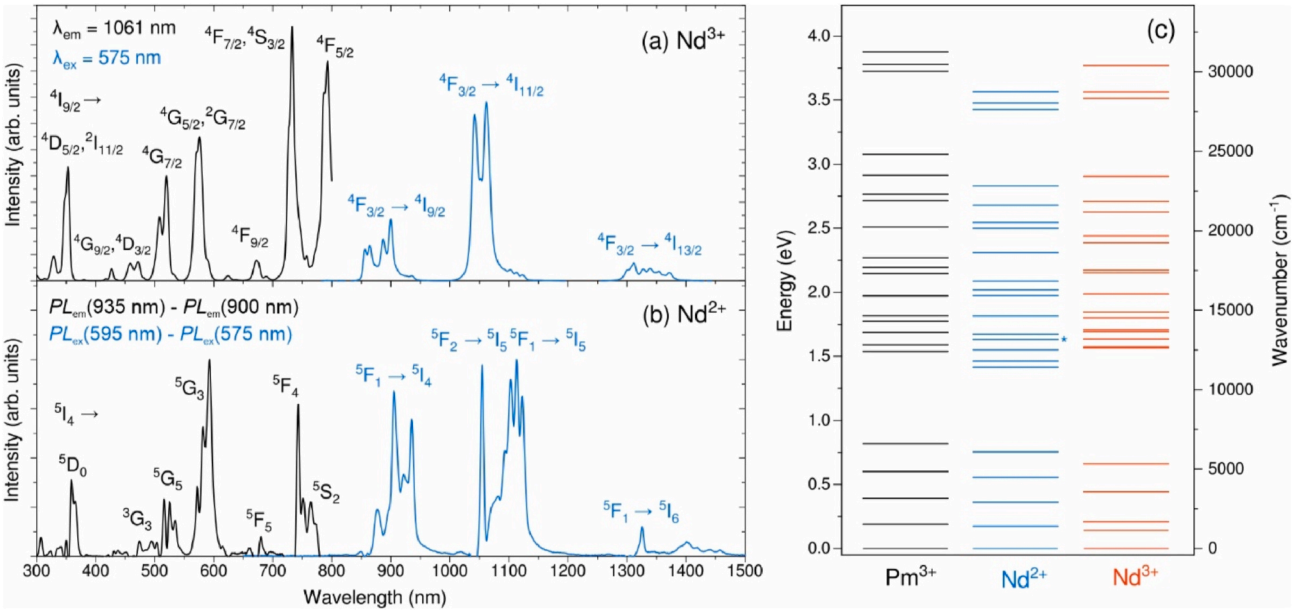

Fig. 3. (a) Photoluminescence excitation and emission spectra where $\lambda_{em} = 1061$ nm and $\lambda_{ex} = 575$ nm, respectively. The intraconfigurational $4f^3 \rightarrow 4f^3$ transitions of Nd^{3+} are labelled. (b) Normalised difference photoluminescence excitation and emission spectra where PL_{em}(935 nm) – PL_{em}(900 nm) and PL_{ex}(595 nm) – PL_{ex}(575 nm), respectively. The intraconfigurational $4f^4 \rightarrow 4f^4$ transitions of Nd^{2+} are labelled. (c) Energy diagrams for Pm^{3+}, as adapted from the literature [26,41], and Nd^{2+} and Nd^{3+} in $NaMgF_3$:Nd. The asterisk marks the predicted position of the first $4f^35d^1$ absorption of Nd^{2+}.

Table 1
Energies of the transitions from the ground state ($^5I_4$) to various excited states for Pm^{3+} in LaF_3:Pm (obtained from Ref. [41]) and Nd^{2+} in $NaMgF_3$:Nd, and from the ground state ($^4I_{9/2}$) to various excited states for Nd^{3+} in $NaMgF_3$:Nd.

Transition $^5I_4 \rightarrow$	Pm^{3+} (from Refs. [26,41]) (eV/nm)	Nd^{2+} (eV/nm)	Transition $^4I_{9/2} \rightarrow$	Nd^{3+} (eV/nm)
$^5S_2$	1.80/688	1.60/774	$^4F_{5/2}$	1.57/792
		1.62/764		1.58/786
		1.65/752		
$^5F_4$	1.83/675	1.67/743	$^4F_{7/2}$	1.69/733
				1.71/727
$^5F_5$	2.00/619	1.82/680	$^4F_{9/2}$	1.85/672
$^5G_3$	2.24/554	2.09/593	$^2H_{11/2}$	1.99/624
		2.13/582		
		2.17/572		
$^5G_5$	2.51/494	2.32/535	$^4G_{5/2}$, $^2G_{7/2}$	2.15/576
		2.36/525		2.17/571
$^3G_3$	2.72/455	2.46/504	$^4G_{7/2}$	2.38/520
		2.51/495		
$^5D_0$	3.72/333	3.39/366	$^2G_{9/2}$	2.44/508
		3.45/359		
			$^4G_{9/2}$, $^2D_{3/2}$	2.63/472
			$^4G_{11/2}$	2.71/458
			$^2D_{5/2}$	2.90/427
			$^4D_{5/2}$	3.51/353
				3.56/348
			$^4D_{7/2}$	3.77/329

Table 2
Compression of the energy levels within the $4f^n$ configurations of Ln^{2+} relative to Ln^{3+} for particular isoelectronic Ln^{2+}/Ln^{3+} pairs in $NaMgF_3$:Ln. †Data for Ho^{3+} were obtained from $KCaF_3$:Ho^{3+} [43] and YAG:Ho^{3+} [44].

Isoelectronic Ln^{2+}/Ln^{3+} pair	Electronic configuration	Atomic number (Ln^{2+}/Ln^{3+})	Compression factor
Nd^{2+}/Pm^{3+}	$4f^4$	60/61	1.087×
Sm^{2+}/Eu^{3+}	$4f^6$	62/63	1.117×
Dy^{2+}/Ho^{3+}	$4f^{10}$	66/67	†1.133×

the difference between the energy of the conduction band of a host compound and the ground state energy of the Ln^{2+} ion in that compound, i.e., the trap depth energy, the more likely that significant concentrations of the Ln^{2+} ion will be observed in Ln-doped compounds [18]. This is readily observed in the various $NaMgF_3$:Ln compounds, where the Ln^{2+} ions with the largest trap depth energies (Eu^{2+} (5.13 eV), Yb^{2+} (4.66 eV), and Sm^{2+} (3.96 eV), in order of decreasing trap depth energy) are observed in significant concentrations, potentially exceeding 10% the total Ln dopant concentration [19,22]. In contrast, Dy^{2+} in $NaMgF_3$:Dy has a trap depth energy of 2.88 eV, and there was no evidence of Dy^{2+} centres in the PL of the compound prior to irradiation [21]. It is interesting that Nd^{2+} was observed in the as-made $NaMgF_3$:Nd samples, as the trap depth energy of Nd^{2+} is lower than that of Dy^{2+} in the compound. It is also interesting that Nd^{2+} 5*d* absorptions were not clearly observed in the PL excitation spectra, where the first 5*d* absorption was predicted to occur at approximately 760 nm [19,45].

It was possible to make a rough estimate of the fraction of total Nd incorporated as Nd^{2+} using the relative peak intensities of the $^4I_4 \rightarrow {}^5F_4$ and $^4I_{9/2} \rightarrow {}^4F_{7/2}$ excitations of the Nd^{2+} and Nd^{3+} ions, respectively, and the oscillator strengths of the same transitions as experimentally determined for $HClO_4$:Ln^{3+} (Ln^{3+} = Pm^{3+}, Nd^{3+}) [46]. The peak intensity of the $^4I_4 \rightarrow {}^5F_4$ excitation was approximately 2% that of the $^4I_{9/2} \rightarrow {}^4F_{7/2}$ excitation. The oscillator strengths of the transitions are given as 2.29×10^6 and 8.9×10^6, respectively [46]. Thus, approximately 8% of the total Nd dopant concentration incorporated as Nd^{2+} in the as-made samples, while the remainder incorporated as Nd^{3+}.

In order to test the predicted electron trapping properties of the Nd^{3+} ion, a sample was exposed to a cumulative X-ray dose of approximately 720 Gy, and luminescence spectra of Nd^{3+} and Nd^{2+} obtained before and after each irradiation. The PL excitation spectra where $\lambda_{em} = 1061$ nm, corresponding to the $^4F_{3/2} \rightarrow {}^4I_{11/2}$ emission of Nd^{3+}, are shown in Fig. 4(a). As expected, the previously attributed Nd^{3+} excitations were observed prior to X-ray exposure. No additional excitations were observed after irradiation. However, the peak intensities of all excitations decreased after irradiation, where the peak intensity of the excitation at 575 nm ($^4I_{9/2} \rightarrow {}^4G_{5/2}$,$^4G_{7/2}$) reduced by 20%. A reduction in the Nd^{3+} PL intensities after irradiation correlates with the expected radiation-induced valence conversion $Nd^{3+} \rightarrow Nd^{2+}$, as the number of

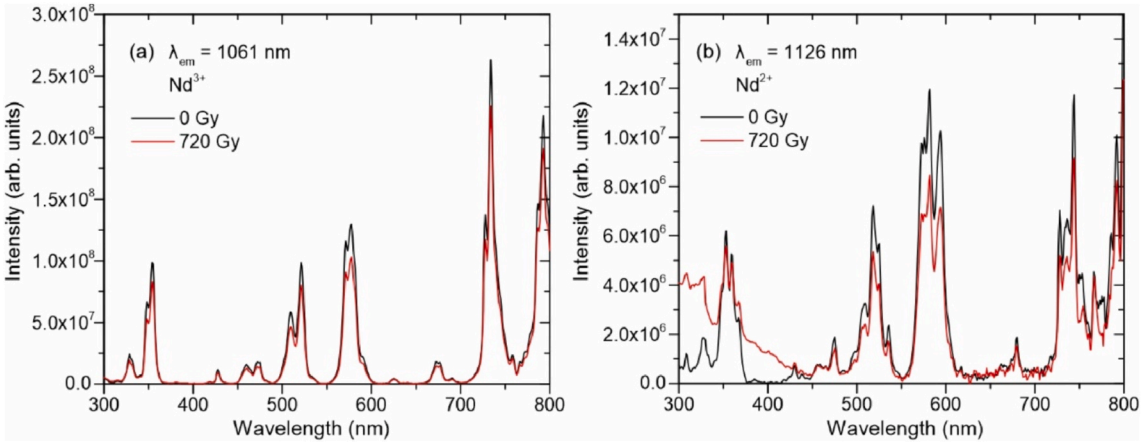

Fig. 4. (a) Photoluminescence excitation spectra where λ_{em} = 1061 nm prior to X-ray exposure (black) and after an X-ray dose of 720 Gy (red). (b) Photoluminescence excitation spectra where λ_{em} = 1126 nm prior to X-ray exposure (black) and after an X-ray dose of 720 Gy (red).

Nd^{3+} sites capable of producing luminescence decreases. The PL excitation spectra where λ_{em} = 1126 nm, corresponding to the Nd^{2+} $^5F_1 \rightarrow {}^5I_5$ emission, prior to and after X-ray exposure are shown in Fig. 4(b). Prior to irradiation the spectrum was dominated by Nd^{2+} excitations, with weak contributions from Nd^{3+} excitations. After irradiation, the excitation peaks above 450 nm decreased, where the peak intensity of the excitation at 595 nm ($^4I_4 \rightarrow {}^5G_3$) was reduced by 30%. The reduction in the Nd^{2+} PL intensities after irradiation is inconsistent with the typical radiation-induced $Ln^{3+} \rightarrow Ln^{2+}$ conversion process seen in similar Ln-doped $NaMgF_3$ compounds [19–21]. However, a broad excitation band appeared at wavelengths below 450 nm after irradiation that could be due to newly created Nd^{2+} sites or radiation-induced defects that yield Nd^{2+} emissions via energy transfer or optically stimulated luminescence. The energy of the band is much greater than the predicted lowest energy Nd^{2+} 5*d* band (760 nm), though it is possible that the band represents higher energy 5*d* absorptions.

The PL emission spectra where λ_{ex} = 400 nm, corresponding to an excitation into the radiation-induced band in the Nd^{2+} excitation spectrum (Fig. 4(b)) where no significant Nd^{2+} or Nd^{3+} $4f^n \rightarrow 4f^n$ excitations exist, are shown in Fig. 5, prior to irradiation and after exposure to total X-ray doses of 360 Gy and 720 Gy. Prior to irradiation, only weak Nd^{3+} emissions were observed. After irradiation, the emission spectra were dominated by Nd^{2+} emissions that increased in intensity after successive irradiations. The specific mechanism via which the Nd^{2+} emissions occur is unclear. As the radiation-induced excitation resembles that attributed to F-centres in $NaMgF_3$ [20,38], it may be that hole-trapping sites preferentially form nearby the existing Nd^{2+} ions, such that irradiation produces semi-localised ($Nd^{2+} + h^+$) centres. Upon stimulation into the F-centre band, electrons released from fluorine vacancies may recombine with the trapped holes, resulting in Nd^{2+} emissions that decrease in intensity during the stimulation period. If the excitation arises from higher energy 5*d* states of newly converted Nd^{2+}, then excitation into this band should revert the Nd^{2+} back to Nd^{3+}, where the Nd^{2+} trap depth is predicted to be 2.72 eV (455 nm). To test these hypotheses, the irradiated sample was stimulated with 400 nm light and the emission at 1126 nm monitored over 3000 s (Fig. 5 inset). The Nd^{2+} emission intensity decreased over time, indicating that the Nd^{2+} radiophotoluminescence was optically bleached, and demonstrating that the radiation-induced changes to the luminescence were optically reversible. Consequently, $NaMgF_3$:Nd could find applications in radiation dose detection and optical information storage.

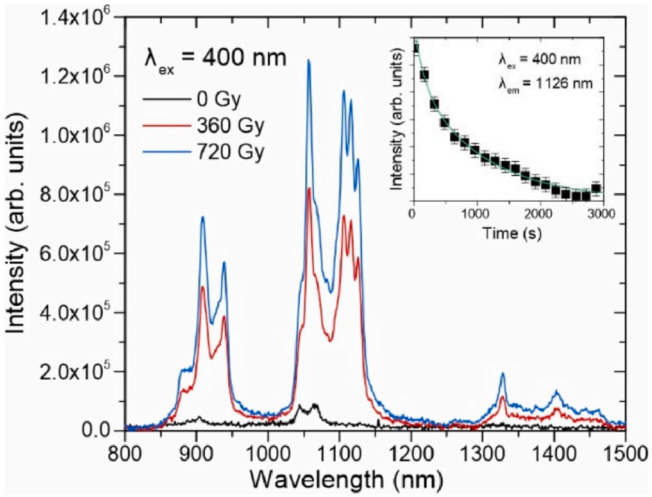

Fig. 5. Photoluminescence emission spectra where λ_{ex} = 400 nm prior to X-ray exposure (black), and after total X-ray doses of 360 Gy (red) and 720 Gy (blue). Inset: Photoluminescence intensity over time, where λ_{ex} = 400 nm and λ_{em} = 1126 nm (black squares). The green line is a guide to the eye.

4. Conclusion

In conclusion, we observed luminescence features in $NaMgF_3$:Nd that were attributed to Nd^{2+}, alongside standard Nd^{3+} emissions. The observation of divalent Nd in compounds is relatively rare, and luminescence properties of Nd^{2+} are not well understood, especially regarding the various intraconfigurational $4f^4 \rightarrow 4f^4$ transitions of the ion. We reported on the synthesis of Nd-doped $NaMgF_3$, where $NaMgF_3$ is known to be a valuable host compound in the study of divalent lanthanides. We demonstrated that the majority of the Nd dopant incorporated into the host compound in the trivalent state, where the Nd^{3+} ion exhibited photoluminescence line emissions over the range 840 nm–1390 nm with corresponding line excitations over the range 300 nm–800 nm, all of which were attributed to specific $4f^3 \rightarrow 4f^3$ transitions. Additional, weaker photoluminescence excitations and emissions were observed over similar wavelength ranges that could not be attributed Nd^{3+} ions. Via comparison with the electronic structure of the seldom studied isoelectronic Pm^{3+} ion the additional photoluminescence features were attributed to a small concentration (<10% of total Nd) of Nd^{2+} ions that incorporated during synthesis. The Nd^{2+} photoluminescence features were directly correlated with the transitions of Pm^{3+} such that the various $4f^4 \rightarrow 4f^4$ transition energies were attributed to particular Nd^{2+} states. The $4f^4$ energy levels were compressed by a factor of 1.09×, relative to those of the Pm^{3+} ion, where the compression was due to the lower effective nuclear charge of Nd^{2+}. This compression factor was compared to those seen in similar divalent-

trivalent isoelectronic pairs, where it was demonstrated that the compression factor increases with atomic number. X-ray irradiation resulted in decreased photoluminescence intensities from both Nd^{3+} and Nd^{2+} when exciting into the $4f^n$ levels. A broad Nd^{2+} excitation appeared below 450 nm after irradiation, such that the Nd^{2+} emission intensities increased for higher energy optical stimulations. Continuous stimulation into the radiation-induced band resulted in a reduction of the Nd^{2+} emissions, demonstrating that the radiation-induced changes are optically reversible. Ultimately, we obtained valuable spectral information related to the infrequently observed Nd^{2+} ion that will provide a reference for fingerprinting the ion in alternative hosts, and a reference for the isoelectronic Pm^{3+} ion. Finally, the radiation-induced changes to the Nd^{2+} luminescence indicate that the compound may find applications in luminescence dosimetry and optical information storage.

Author statement

J. J. Schuyt: Conceptualization, Methodology, Investigation, Writing – original draft, Writing – review & editing. G. V. M. Williams: Conceptualization, Methodology, Writing – review & editing.

Declaration of competing interest

The authors declare that they have no known competing financial interests or personal relationships that could have appeared to influence the work reported in this paper.

Acknowledgements

We acknowledge funding support from the New Zealand Ministry of Business, Innovation and Employment (RTVU2102) and the MacDiarmid Institute for Advanced Materials and Nanotechnology.

References

[1] A. Ikesue, Polycrystalline Nd:YAG ceramics lasers, Opt. Mater. 19 (2002) 183–187.
[2] J.L. Leano Jr., M. Fang, R. Liu, Review - narrow-band emission of nitride phosphors for light-emitting diodes: perspectives and opportunities, ECS J. Solid State Sci. Technol. 7 (2018) R3111.
[3] X. Qin, X. Liu, W. Huang, M. Bettinelli, X. Liu, Lanthanide-activated phosphors based on 4f-5d optical transitions: theoretical and experimental aspects, Chem. Rev. 117 (2017) 4488.
[4] L.C. Dixie, A. Edgar, C.M. Bartle, Samarium doped calcium fluoride: a red scintillator and X-ray phosphor, Nucl. Instrum. Methods Phys. Res. 753 (2014) 131–137.
[5] G. Tian, Z. Gu, L. Zhou, W. Yin, X. Liu, L. Yan, S. Jin, W. Ren, G. Xing, S. Li, Y. Zhao, Mn^{2+} dopant-controlled synthesis of $NaYF_4$:Yb/Er upconversion nanoparticles for in vivo imaging and drug delivery, Adv. Mater. 24 (2012) 1226–1231.
[6] R.H.J. Fastenau, E.J.v. Loenen, Applications of rare earth permanent magnets, J. Magn. Magn Mater. 157/158 (1996) 1–6.
[7] B. Henderson, G.F. Imbusch, Optical Spectroscopy of Inorganic Solids, Oxford University Press, New York, 2006.
[8] G.H. Dieke, H.M. Crosswhite, The spectra of the doubly and triply ionized rare earths, Appl. Opt. 2 (1963) 675.
[9] M. Suta, C. Wickleder, Synthesis, spectroscopic properties and applications of divalent lanthanides apart from Eu^{2+}, J. Lumin. 210 (2019) 210–238.
[10] P. Dorenbos, The 5d level positions of the trivalent lanthanides in inorganic compounds, J. Lumin. 91 (2000) 155–176.
[11] M. Karbowiak, C. Rudowicz, J. Cichos, Extension of high-resolution optical absorption spectroscopy to divalent neodymium: absorption spectra of Nd^{2+} ions in a $SrCl_2$ host, Angew. Chem. Int. Ed. 56 (2017) 10721.
[12] P. Dorenbos, Thermal quenching of Eu^{2+} 5d-4f luminscence in inorganic compounds, J. Phys. Condens. Matter 17 (2005) 8103–8111.
[13] N.R.J. Poolton, A.J.J. Bos, P. Dorenbos, Luminescence emission from metastable Sm^{2+} defects in YPO_4:Ce,Sm, J. Phys. Condens. Matter 24 (2012) 225502.
[14] C. MacKeen, F. Bridges, M. Kozina, A. Mehta, M.F. Reid, J.P.R. Wells, Z. Barandiaran, Evidence that the anomalous emission from CaF_2:Yb^{2+} is not described by the impurity trapped exciton model, J. Phys. Chem. Lett. 8 (2017) 3313–3316.
[15] R.B. Hughes-Currie, K.V. Ivanovskikh, M.F. Reid, J.R. Wells, R.J. Reeves, A. Meijerink, Vacuum ultraviolet synchrotron measurements of excitons in $NaMgF_3$:Yb^{2+}, J. Lumin. 169 (2016) 419–421.
[16] L.C. Dixie, A. Edgar, M.F. Reid, Sm^{2+} fluorescence and absorption in cubic $BaCl_2$: strong thermal crossover of fluorescence between $4f^6$ and $4f^55d^1$ configurations, J. Lumin. 132 (2012) 2775–2782.
[17] P. Dorenbos, Energy of the Eu^{2+} 5d state relative to the conduction band in compounds, J. Lumin. 128 (2008) 578–582.
[18] P. Dorenbos, Lanthanide charge transfer energies and related luminescence, charge carrier trapping, and redox phenomena, J. Alloys Compd. 488 (2009) 568–573.
[19] J.J. Schuyt, G.V.M. Williams, Oxygen-impurity charge transfer in $NaMgF_3$:Ln (Ln = Yb, Sm, or Eu): establishing the lanthanide energy levels in $NaMgF_3$, J. Lumin. 211 (2019) 413–417.
[20] J.J. Schuyt, G.V.M. Williams, Radiation-induced changes in the optical properties of $NaMgF_3$(Sm): observation of resettable Sm radio-photoluminescence, Mater. Res. Bull. 106 (2018) 455–458.
[21] J.J. Schuyt, G.V.M. Williams, Photoluminescence of Dy^{3+} and Dy^{2+} in $NaMgF_3$:Dy: a potential infrared radiophotoluminescence dosimeter, Radiat. Meas. 134 (2020) 106326.
[22] J.J. Schuyt, J. Donaldson, G.V.M. Williams, S.V. Chong, Modelling the radioluminescence of Sm^{2+} and Sm^{3+} in the dosimeter material $NaMgF_3$:Sm, J. Phys. Condens. Matter 32 (2020), 025703.
[23] J.J. Schuyt, G.V.M. Williams, Quenching of the Sm^{2+} luminescence in $NaMgF_3$:Sm via photo-thermal ionization: alternative method to determine divalent lanthanide trap depths, Appl. Phys. Lett. 115 (2019) 181104.
[24] M.K.V. Elkina, Promethium: to strive, to seek, to find and not to yield, Front. Chem. 8 (2020) 588.
[25] M.D. Shinn, W.F. Krupke, R.W. Solarz, T.A. Kirchoff, Spectroscopic and laser properties of Pm^{3+}, IEEE J. Quant. Electron. 24 (1988) 1100.
[26] W.T. Carnall, Energy level analysis of Pm^{3+}:$LaCl_3$, J. Chem. Phys. 64 (1976) 3582.
[27] D.S. McClure, Survey of the spectra of the divalent rare-earth ions in cubic crystals, J. Chem. Phys. 39 (1963) 3251.
[28] T. Sizova, E. Radzhabov, R. Shendrik, A. Egranov, A. Shalaev, Study of Nd^{2+} absorption in x-irradiated CaF_2, SrF_2, BaF_2 crystals, Radiat. Meas. 90 (2016) 68–70.
[29] H. Hayashi, M. Akabori, T. Ogawa, K. Minato, Spectrophotometric study of Nd^{2+} ions in LiCl-KCl eutectic melt, Z. Naturforsch. 59 (2004) 705.
[30] W. Xu, J.R. Peterson, Stablization of divalent neodymium (Nd^{2+}) in strontium tetraborate, J. Alloys Compd. 249 (1997) 213.
[31] M. Karbowiak, C. Rudowicz, Trends in Hamiltonian parameters determined by systematic analysis of f-d absorption spectra of divalent lanthanides in alkali-halides hosts and supported by first calculations of the Nd^{2+} electronic structure: I. $SrCl_2$:Ln^{2+}, J. Lumin. 199 (2018) 116.
[32] M. Karbowiak, C. Rudowicz, Optical absorption spectra of divalent neodymium (Nd^{2+}) in bromide and iodide hosts, Eur. J. Inorg. Chem. 2018 (2018) 1660–1669.
[33] R.Y. Abdulsabirov, M.L. Falin, I.I. Fazlizhanov, B.N. Kazakov, S.L. Korableva, I. R. Ibragimov, G.M. Safiullin, Z.S. Yakovleva, EPR and optical spectroscopy of neodymium ions in $KMgF_3$ and $KZnF_3$ crystals, Appl. Magn. Reson. 5 (1993) 377.
[34] S. Mukherjee, N. Pathak, D. Das, D. Dutta, Engineering defect clusters in distorted $NaMgF_3$ perovskite and their important roles in tuning the emission characteristics of Eu^{3+} dopant ion, RSC Adv. 11 (2021) 5815.
[35] S. Lizzo, A. Meijerink, G.J. Dirksen, G. Blasse, On the luminescence of divalent ytterbium in $KMgF_3$ and $NaMgF_3$, J. Phys. Chem. Solid. 56 (1995) 959–964.
[36] J.C. Gacon, A. Gros, H. Bill, J.P. Wicky, New measurements of the emission spectra of Sm^{2+} in $KMgF_3$ and $NaMgF_3$ crystals, J. Phys. Chem. Solid. 42 (1981) 587–593.
[37] R.D. Shannon, Revised effective ionic radii and systematic studies of interatomic distances in halides and chaleogenides, Acta Crystallogr. 32 (1976) 751.
[38] J.J. Schuyt, G.V.M. Williams, F-centre/Mn complex photoluminescence in the fluoroperovskites $AMgF_3$:Mn (A = Na, K, or Rb), Opt. Mater. 1 (2019) 100010.
[39] A. Sousa, A. Souza, H. Lima, Defect clustering in an Eu-doped $NaMgF_3$ compound and its influence on luminescent properties, Mater. Adv. 2 (2021) 1378.
[40] D.C. Yu, X.Y. Huang, S. Ye, Q.Y. Zhang, J. Wang, A sequential two-step near-infrared quantum splitting in Ho^{3+} singly doped $NaYF_4$, AIP Adv. 1 (2011), 042161.
[41] W.T. Carnall, G.L. Goodman, K. Rajnak, R.S. Rana, A systematic analysis of the spectra of the lanthanides doped into single crystal LaF_3, J. Chem. Phys. 90 (1989) 3443.
[42] G.V.M. Williams, S. Janssens, C. Gaedtke, S.G. Raymond, D. Clarke, Observation of photoluminescence and radioluminescence in Eu and Mn doped $NaMgF_3$ nanoparticles, J. Lumin. 143 (2013) 219–225.
[43] M.A. Mondragon, J. Garcia M, W.A. Sibley, C.A. Hunt, Optical absorption and emission from Ho^{3+} ions in $KCaF_3$ crystals, J. Solid State Chem. 76 (1988) 368.
[44] M. Malinowski, Z. Fukacz, M. Szuflinska, A. Wnuk, M. Kaczkan, Optical transitions of Ho^{3+} in YAG, J. Alloys Compd. 300–301 (2000) 389–394.
[45] P. Dorenbos, Improved parameters for the lanthanide $4f^q$ and $4f^{q-1}5d$ curves in HRBE and VRBE schemes that takes the nephelauxetic effect into account, J. Lumin. 222 (2020) 117164.
[46] W.T. Carnall, P.R. Fields, K. Rajnak, Energy Levels and Intensities in the Solution Absorption Spectra of the Trivalent Lanthanides, Argonne National Laboratory - Technical Report, 1968.